

Improved predictions of the physical properties of Zn- and Cd-based wide band-gap semiconductors: A validation of the ACBN0 functional

Priya Gopal,^{1,2} Marco Fornari,^{1,2,*} Stefano Curtarolo,^{2,3} Luis A. Agapito,^{2,4}
Laalitha S. I. Liyanage,^{2,4} and Marco Buongiorno Nardelli^{2,4,†}

¹*Department of Physics, Central Michigan University, Mt. Pleasant, Michigan 48859, USA*

²*Center for Materials Genomics, Duke University, Durham, North Carolina 27708, USA*

³*Materials Science, Electrical Engineering, Physics and Chemistry, Duke University, Durham, North Carolina 27708, USA*

⁴*Department of Physics, University of North Texas, Denton, Texas 76203, USA*

(Received 26 February 2015; revised manuscript received 1 May 2015; published 4 June 2015)

We study the physical properties of ZnX ($X = O, S, Se, Te$) and CdX ($X = O, S, Se, Te$) in the zinc-blende, rock-salt, and wurtzite structures using the recently developed fully *ab initio* pseudohybrid Hubbard density functional ACBN0. We find that both the electronic and vibrational properties of these wide band-gap semiconductors are systematically improved over the PBE values and reproduce closely the experimental measurements. Similar accuracy is found for the structural parameters, especially the bulk modulus. ACBN0 results compare well with hybrid functional calculations at a fraction of the computational cost.

DOI: [10.1103/PhysRevB.91.245202](https://doi.org/10.1103/PhysRevB.91.245202)

PACS number(s): 71.15.Mb, 71.20.Nr, 05.30.Fk, 71.15.Ap

I. INTRODUCTION

Among II-VI semiconductors, oxides and chalcogenides with Cd and Zn are the subject of extensive scrutiny for their potential applications in spintronics, optoelectronics, and photovoltaics [1]. These applications rely on heterojunctions, quantum dots, and other nanostructures where the delicate interplay between structural and electronic properties must be carefully captured to understand and improve the device's performance. Common computational approaches based on density functional theory (DFT), however, fall short when trying to predict accurate structural and electronic properties, greatly limiting the development process.

In DFT, most of the calculations involving II-VI semiconductors and oxides use the exchange-correlation (xc) potential within the local density approximation (LDA) or the generalized gradient approximation (GGA) [2,3]. While the DFT-LDA/GGA method provides reasonable predictions for structural properties, it fails dramatically in describing the electronic properties, especially the band gaps, which are underestimated by 50% or more with respect to experimental values. In ZnO, for instance, the calculated band gap is 0.8 eV, while the experimental value is 3.44 eV [4,5]; CdO is described as a semimetal [6], whereas experimentally rock salt CdO has an indirect band gap of 0.9 eV [7]. Similar discrepancies in the calculated and measured band gaps are found in the chalcogenides as well [8,9]. In the case of Cd and Zn oxides and chalcogenides, in addition, the energy of the occupied *d* manifold is found about 3 eV higher than the experimental value and leads to fictitious *d-p* mixing in the valence band [8,9].

The limitations mentioned above are a consequence of the lack of self-interaction corrections [2] and of the derivative discontinuity in the exchange-correlation energy [10–12] in all traditional functionals such as LDA or PBE-GGA. Clearly only the inclusion of nonlocal correlations and nonlocal Hartree-

Fock (HF) exchange can, in part, alleviate these problems. A number of approaches have been proposed to overcome these deficiencies, among which: LDA plus self-interaction (LDA-SIC) [2], self-interaction-relaxation correction (SIRC-LDA) [8], DFT+*U* [13,14], different versions of the *GW* approximation [15–17], and hybrid functionals [18,19]. Among these approaches, the ones that have gained more traction in recent years are the DFT+*U* [13,14] and hybrid functionals [18,19].

In DFT+*U* one introduces on-site Coulomb and exchange interaction terms *U* and *J* to account for the localization of *d* states. The on-site orbital-dependent parameters *U* and *J* correspond to the Coulomb and exchange couplings between electrons of a particular angular momentum that are localized on the same atom. The appeal of DFT+*U* relies on its effectiveness and low computational cost in correcting for the over-delocalization of the *d* electrons in transition metal ions. Although the original DFT+*U* formulation is rigorous, in most cases *U* and *J* are treated as empirical adjustable parameters which are often obtained by fitting the band structure to available experimental values [20]. This approach requires fitting information from experimental data and its predictive value for new materials and heterostructures is limited. There are a few common *ab initio* methods to derive *U* and *J* such as the constrained LDA (cLDA) [21] and linear response approach [22,23]. These methods are, unfortunately, computationally expensive, often requiring large supercell calculations. Moreover, although the linear response method has been widely used for open-shell systems, it is not suitable for closed-shell elements such as Zn and Cd, where the localized bands are completely full and insensitive to linear perturbations [20].

Hybrid functionals are based on the idea of computing the exact exchange energy from the Kohn-Sham wave functions and to mix it with the (semi)local approximation of correlation energy of DFT [24]. In this respect, the method does not suffer any limitations in dealing with closed-shell elements and it is very successful in predicting the energy gap for semiconductors and insulators. Clearly some degree of exact exchange is necessary for a more accurate description of the

*marco.fornari@cmich.edu

†mbn@unt.edu

electronic structure. However, also hybrid functionals have a somewhat empirical component, since the level of mixing is not determined from first principles [19].

In order to facilitate the accurate characterization of electronic properties of materials at a low computational cost, a fundamental condition for the development of effective high-throughput quantum-mechanics frameworks for accelerated materials discovery [25–28], some of the authors have recently introduced the ACBN0 functional [29], a pseudohybrid Hubbard density functional that introduces a new *ab initio* approach to compute U and J that does not contain any empirical parameter. In this work we demonstrate that, by using ACBN0, we can improve substantially the predictive value of DFT calculations for the physical properties of Zn and Cd oxides and chalcogenides at a fraction of the computational cost of hybrid functionals. The paper is organized as follows: in Sec. II we briefly discuss the ACBN0 method. In Sec. III we discuss our results for the Zn and Cd chalcogenides by comparing structural, electronic, and vibrational properties with more standard approaches.

II. METHODOLOGY

ACBN0 is based on the DFT+ U energy functional as formulated by Dudarev [30]:

$$E_{\text{DFT}+U} = E_{\text{DFT}} + E_U - E_{\text{DC}},$$

where E_{DFT} is the DFT energy calculated using a LDA or GGA functional, the two parameters U and J have been replaced by an effective on-site Coulomb interaction $U_{\text{eff}} = U - J$, and E_{DC} takes care of the double counting terms in the energy expansion. For technical details on the ACBN0 formalism we refer the reader to Ref. [29].

ACBN0 resolves the ambiguities in DFT+ U by computing on-the-fly the local Coulomb (U) and exchange (J) integrals for the specific orbitals under consideration via a procedure based on an *ad hoc* renormalization of the density matrix. In this way, the value of U_{eff} results a functional of the electron density and depends directly on the chemical environment and the crystalline field.

TABLE I. Converged values of U_{eff} (in eV) for the Zn 3*d* and the anion p states. The calculations were performed at the equilibrium lattice constants in Table III.

	Phase	Zn 3 <i>d</i>	Anion p
ZnO	wz	13.19	5.57
	zb	13.24	6.02
	rs	13.52	6.05
ZnS	wz	13.48	3.50
	zb	13.21	3.42
	rs	14.54	3.76
ZnSe	wz	15.00	2.55
	zb	14.60	2.52
	rs	15.68	2.77
ZnTe	wz	16.00	2.40
	zb	16.89	2.43
	rs	17.08	2.66

TABLE II. Converged values of U_{eff} (in eV) for the Cd 4*d* and the anion p states. The values are for the equilibrium lattice constants in Table III.

	Phase	Cd 4 <i>d</i>	Anion p
CdO	wz	10.69	4.50
	zb	10.49	4.03
	rs	10.73	3.92
CdS	wz	11.07	3.69
	zb	10.89	3.64
	rs	11.77	3.94
CdSe	wz	11.58	2.68
	zb	11.69	2.70
	rs	12.51	3.05
CdTe	wz	12.95	2.57
	zb	13.00	2.55
	rs	13.70	2.46

In traditional formulation of DFT+ U [30] the correction term U was based explicitly on the localization of the d orbitals and was not used for the p or s orbitals which tend to be less localized compared to d electrons. However, in the ACBN0 formulation U_{eff} is computed directly on the chosen Hubbard center from the Coulomb and exchange Hartree-Fock energies of the solid and can be evaluated for any contributing orbital. The evaluation of U_{eff} for any orbital symmetry is not a new concept (see for instance Ref. [31]) but it is particularly relevant for the systems studied in this work.

In the current implementation of ACBN0, U_{eff} is evaluated through a self-consistent procedure where we start by calculating the electronic structure for an initial guess of $U_{\text{eff}}^d = U_{\text{eff}}^p = 0$ eV and converge to U_{eff} within 10^{-4} eV. A plot of the convergence of U_{eff} with the iteration steps is provided in the Supplemental Information [32]. Tables I and II provide the converged U_{eff} values for all the semiconductors studied in this work.

ACBN0 calculations have been done using the QUANTUM ESPRESSO [33] and WanT [34,35] packages with norm-conserving pseudopotentials from the pslibrary1.0 database. A kinetic energy cutoff of 350 Ry and a k -point mesh of $12 \times 12 \times 12$ was used for all total-energy calculations. Hybrid functional DFT calculations were performed using the Vienna *ab initio* simulation package (VASP) [36] with the HSE06 [18]. This functional is defined by replacing 25% of the PBE exchange interaction by a screened nonlocal functional with an inverse screening length of $0.2/\text{\AA}$. A $6 \times 6 \times 6$ Monkhorst-Pack k -point mesh was used and a plane-wave cutoff of 500 eV was used for all the HSE06 calculations.

III. RESULTS

This section discusses the structural, electronic, and vibrational properties of ZnO, ZnS, ZnSe, ZnTe, CdO, CdS, CdSe, and CdTe computed with the ACBN0 functional.

Under standard conditions ZnO is stable in the wurtzite (wz) structure [1], CdO in the rock-salt (rs) structure, while the rest of the compounds are stable in the zinc-blende (zb) structure. Due to the importance of these materials in semiconductor nanostructures such as heterojunctions and quantum dots that

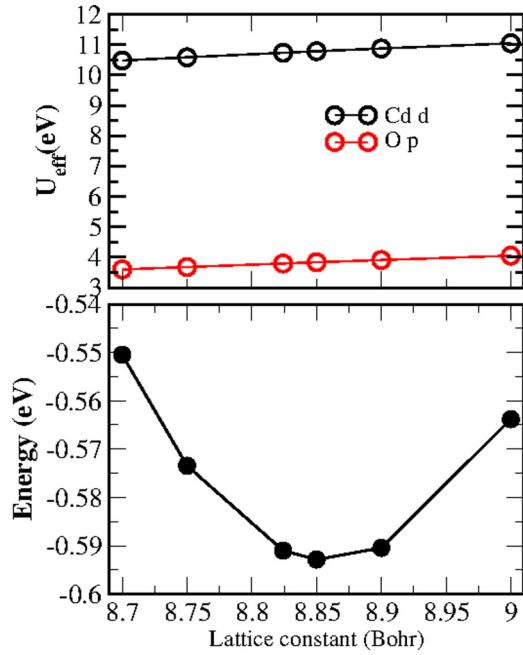


FIG. 1. (Color online) Lower panel: Energy-volume curve of CdO in the rs phase as calculated by the ACBN0 functional. Upper panel: Variation of the converged U_{eff} of Cd and O in CdO as a function of lattice constant.

are usually grown epitaxially with far-from-the-equilibrium techniques, we study all three competing phases for all the chemical compositions. These different structures can be

stabilized by alloying and epitaxial strain. Results not reported in the paper can be found in the Supplemental Material [32].

A. Structural properties

The lattice constants (a_0) and bulk moduli (B) for each of the II-VI semiconductors in the three bulk phases are obtained by fitting the total energy as a function of volume to the Murnaghan's equation of state (eos). As discussed in Sec. II, U_{eff} is a functional of the electron density and is thus dependent on the geometry of the ground state. For a small volume change around equilibrium, the calculated U_{eff} varies linearly with the volume. As an example, at the top of Fig. 1 we have plotted the variation of U_{eff} for CdO in the rs phase where we observe the linear scaling for both the Cd's and the O's U_{eff} , most likely related to bond length changes that affect the wave-functions overlap and the electron localization.

In Tables III and IV we have listed all the values of the computed lattice constants and bulk moduli of all the II-VI semiconductors in the three phases using PBE, HSE, and ACBN0 (and SIRC, whenever available) with references to existing experimental values. Experimentally, the lattice constants follow the trend of $\text{ZnO} < \text{ZnS} < \text{ZnSe} < \text{ZnTe}$ and similarly for the CdX series. This trend of increasing lattice constant is described in the PBE, HSE, and ACBN0 functionals. The experimental bulk moduli shows a reverse trend, i.e., the bulk modulus decreases as we go from O to S to Se to Te.

In Figs. 2(a) and 2(b) we have plotted the relative percentage error of the three functionals PBE, HSE, and ACBN0 in

TABLE III. Comparison of the lattice constants for the different compounds calculated using ACBN0 and other functionals. All the PBE and HSE values are computed in this work. For wz, the first value is the in-plane lattice parameter a and the second value is the out-of-plane lattice parameter c . All the SIRC values reported here are taken from Ref. [8].

System	Phase	PBE	HSE	SIRC	ACBN0	Experiment
ZnO	wz	3.283, 5.309	3.260, 5.221	3.290, 5.29	3.270, 5.164	3.258, 5.220 [39]
	zb	4.670	4.582		4.580	4.620 [40,41]
	rs	4.370	4.278		4.289	4.272 [41,42]
ZnS	wz	3.880, 6.300	3.850, 6.271	3.830, 6.280	3.851, 6.278	3.811, 6.234 [43]
	zb	5.489	5.432	5.421	5.437	5.410 [39]
	rs	5.143	5.077		5.080	5.060 [43,44]
ZnSe	wz	4.043, 6.70	4.030, 6.620		4.020, 6.630	3.980, 6.530 [8,39]
	zb	5.771	5.708		5.696	5.667 [39,45]
	rs	5.401	5.330		5.321	
ZnTe	wz	4.366, 7.176	4.35, 7.132		4.340, 7.140	4.320, 7.100 [46]
	zb	6.199	6.154		6.148	6.089 [8,45]
	rs	5.788	5.743		5.732	
CdO	wz	3.700, 5.850	3.650, 5.800		3.590, 5.750	
	zb	5.172	5.103		5.054	
	rs	4.771	4.722	4.781	4.689	4.696 [6,47,48]
CdS	wz	4.206, 6.85	4.223, 6.951	4.154, 6.762	4.183, 6.682	4.135, 6.701 [43,49]
	zb	5.963	5.901	5.851	5.892	5.820 [39,43,50]
	rs	5.890	5.466		5.459	
CdSe	wz	4.39, 7.1	4.350, 7.112	4.292, 7.021	4.33, 7.072	4.310, 7.010 [8]
	zb	6.239	6.158	6.071	6.142	6.084 [8]
	rs	5.800	5.697		5.680	
CdTe	wz	4.550, 7.451	4.580, 7.460		4.600, 7.498	
	zb	6.621	6.571	6.401	6.560	6.480 [45]
	rs	6.130	6.092		6.076	

TABLE IV. Comparison of the bulk moduli B (GPa) of different compounds using three different functionals. All the PBE and HSE values are calculated in this work.

System	Phase	PBE	HSE	SIRC	ACBN0	Experiment
ZnO	wz	127	143	159	157	136–183 [8,39,41]
	zb	123	143		162	
	rs	156	188		205	177–228 [41]
ZnS	wz	60	74	81	79	76 [51]
	zb	68	74.4	81	80	76.9 [39]
	rs	84	95.4		101.6	103.6 [44]
ZnSe	wz	57	62.69		64	
	zb	55.8	61		66.3	65.7 [45]
	rs	70	78		66.8	
ZnTe	wz	45	58.46		56	
	zb	43	47.19		49.4	50.9 [8,45]
	rs	53.3	58.82		60	
CdO	wz	92.7	104		114	
	zb	91	102		124	
	rs	119	137	152	170	147 [52]
CdS	wz	54	57	74	53	61 [8], 65 [43]
	zb	53.5	58.94	70	63.3	55 [43]
	rs	63.3	78.6		83.2	
CdSe	wz	48	50.80	62	52	55
	zb	41.5	49.7	66	53.4	45.1 [43]
	rs	53	67.4		64	
CdTe	wz	55	60		57.4	
	zb	57	38.4	52	42	42 [39]
	rs	45	51.86		53.1	

predicting the lattice constants and bulk moduli with respect to the measured values. In the plot we have included only the stable phases for each of the eight semiconductors since we did not have experimental data on the nonequilibrium phases. The values for the other three phases for the II-VI semiconductors are listed in Table III. Except for CdO and ZnO, all the other semiconductors have a stable zb structure. For ZnO, we have listed the error for one of the lattice parameters a , while for CdO we have used the rs phase.

The lattice constants and bulk moduli are more accurately described by HSE and ACBN0 compared to PBE functional calculations. The PBE overestimates the lattice constants significantly (up to 2%) as seen in Fig. 2(a) and severely underestimates the bulk moduli [see Fig. 2(b)]; in some cases the error is more than 50% compared to the experimental value. The HSE functional shows a better improvement in the prediction of lattice constants reducing the error to less than 1%. The lattice constants predicted by the ACBN0 follow the HSE closely with an error less than 1%. Note that the ACBN0 preserves the accuracy of the HSE calculations with 8–10 times speed up in terms of calculation time.

The bulk modulus predicted by ACBN0 shows a tremendous improvement over both the HSE and the PBE functional. In CdS, CdSe, and CdTe the agreement with experimental values is exceptional with an error less than (0.5%). Note that the PBE error in the bulk moduli are greater than 20%. These results indicates that using ACBN0 for the calculations of phonon spectra or any lattice dynamical property will yield much improved results, as already observed in the case of

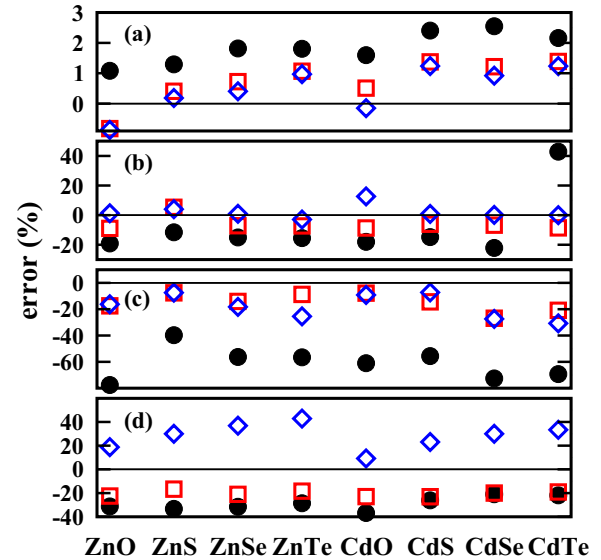


FIG. 2. (Color online) Comparison of percentage relative error in the predictions of (a) lattice constants, (b) bulk moduli, (c) band gap, and (d) energies of the d band calculated using PBE, HSE, and ACBN0 functionals. All the absolute values are listed in Tables III–V. The errors are calculated relative to the experimental values in Tables III–V. In cases where there is more than one experimental value, we take the average of the minimum and the maximum value as the reference experimental value. Comparison is made only for the stable phases of the II-VI compounds. Black circles are the PBE values, open red squares are the HSE values, and open blue diamonds are the ACBN0 values. The experimental values are referenced by the black solid line at 0.

ZnO [37], where the values of the Zn and O U_{eff} , originally fitted to reproduce the experimental band gap and position of the d bands, are in remarkable agreement with the ones predicted by ACBN0. Incidentally, U_{eff} values fitted to HSE calculations have been proposed in the past for ZnO and ZnS [31,38]. While for ZnO the values are again close to our predictions, the values for ZnS are very much different. See Sec. III C for a comprehensive discussion of the lattice dynamical properties of these systems.

For all other phases, the ACBN0 functional reproduces the HSE values closely as seen in Tables III and IV at a much lower computational cost. Overall the structural properties of the II-VI semiconductors computed with the ACBN0 functional show better agreement with respect to experimental results.

B. Electronic properties

The band structures of the eight semiconductors in all three different crystal phases were computed to assess the veracity of the ACBN0 functional in the prediction of band gaps. For comparison we computed the band structures within the PBE and the HSE functionals. All the band structures were calculated at the theoretical equilibrium volume optimized within each functional. In the wz and zb compounds, the band gap is direct while in the rs compounds the gap is indirect between the L and Γ point. A summary of the values of the energy gaps (E_g) for the different compounds is presented in Table V as calculated by the ACBN0, PBE,

TABLE V. Comparison of the energy gaps (E_g) in eV for the different compounds using three different functionals. All the PBE and HSE values are calculated in this work. In the rs phase, two values are listed. The first one is the direct band gap (Γ - Γ) while the second one in parentheses is the indirect band gap between L and Γ point. For the zb and wz phases, the gap is direct from Γ - Γ . The experiment values are reported whenever available.

System	Phase	PBE	HSE	SIRC	ACBN0	Experiment
ZnO	wz	0.85	2.90		2.91	3.2 [39], 3.4 [41]
	zb	0.59	2.70		2.74	3.27 [40]
	rs	2.17(0.89)	4.35(2.90)		4.17(3.09)	4.5(2.45) [53]
ZnS	wz	2.10	3.42, 3.34 [54]	3.6	3.31	3.86 [51], 3.91 [55]
	zb	2.23	3.49 [56]	3.6	3.42	3.7 [21], 3.66 [45]
	rs	2.1(0.83)	3.7(1.31)		3.52(1.28)	
ZnSe	wz	1.27	2.46		1.90	2.87 [45]
	zb	1.18	2.32 [45], 2.42 [56]	2.1	2.041	2.70 [45]
	rs	1.4(<0)	2.60(<0)		2.02(<0)	
ZnTe	wz	1.17	2.22		1.82	
	zb	1.043	2.36 [56], 2.19 [45]	1.4	1.79	2.38 [45]
	rs	0.6	1.4		1.2	
CdO	wz	<0	0.75, 1.13 [57]		1.23	0.91 [58]
	zb	<0	1.04		1.35	
	rs	0.85(<0)	2.01(0.89)		1.98(0.70)	2.18–2.23(0.9–1.08) [48,59]
CdS	wz	1.36	2.15, 2.09 [49]	2.5	2.4	2.5 [60]
	zb	1.11	2.13	2.4	2.3	2.55 [45], 2.4 [8]
	rs	1.71(<0)	2.9(1.4)		2.95(1.27)	1.5 [45]
CdSe	wz	0.73	1.77	1.3	1.61	1.8 [8]
	zb	0.52	1.39	1.4	1.38	1.90 [45], 1.82 [8]
	rs	<0	0.69(<0)		1.4(0.3)	
CdTe	wz	0.64	1.6		1.33	1.8
	zb	0.58	1.51, 1.52 [61], 1.67 [56]	0.8	1.43	1.92 [45], 1.61 [61]
	rs	<0	1.4(<0)		1.3(<0)	

and HSE functionals along with references to the SIRC and experimental values whenever available.

Experimentally, the band gap in both the ZnX and the CdX series decreases with increasing lattice constants, i.e., the band gap decreases as we proceed from S to Se to Te. Both ZnO and CdO show the anomaly of a lower band gap compared to ZnS and CdS, respectively, in spite of a lower lattice constant. This trend of decreasing band gap is described by all the functionals: PBE, HSE, and ACBN0. The absolute value of the band gap, however, is severely underestimated by PBE: in the oxides, especially, we see an error bar of more than 60% [see Fig. 2(c)]. The ACBN0 functional reduces this error to less than 20%. The band gaps predicted by ACBN0 for the eight semicon-

ductors studied here lie within 0.5 eV of the experimental value.

Before discussing the similarities of the HSE and the ACBN0 functionals, we first look at the general features of the calculated band structures. Representative band structures for the eight semiconductors in their stable phases calculated with the ACBN0 and the PBE functionals are shown in Figs. 3 and 4 (band structure of all the other phases are compiled in the Supplemental Material [32]). Within PBE (black lines), the overall band profiles are very similar in both the ZnX and CdX series. The lowest energy manifolds (below -10 eV) are rather narrow and entirely of s character. At higher energy we found the bands derived from the d orbitals

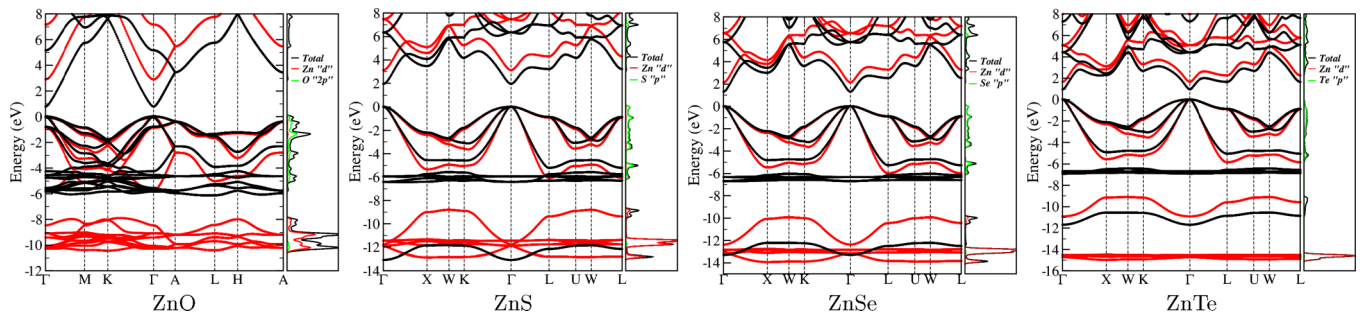


FIG. 3. (Color online) Band structure of ZnX ($X = O, S, Se, Te$) within the ACBN0 (red lines) method for the stable wz and zb phase. The PBE (black lines) band structure is also shown for comparison. Brillouin zone integration follows the AFLOW standard as discussed in Ref. [63].

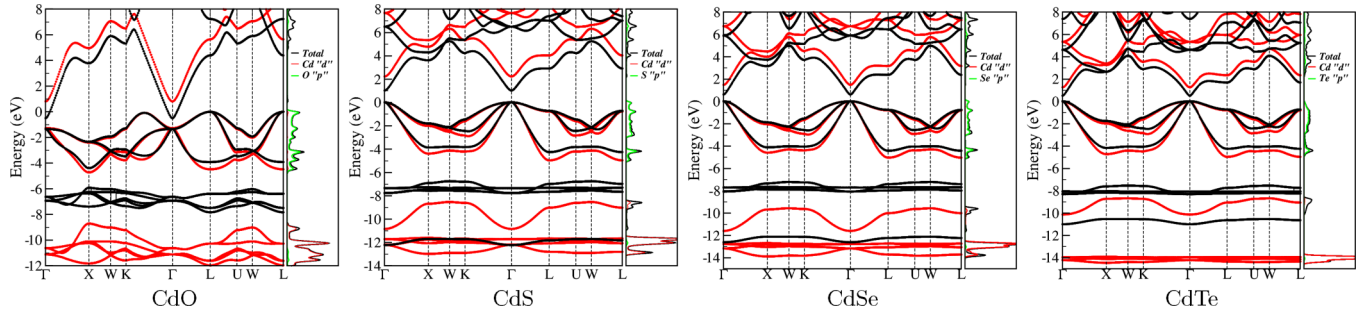


FIG. 4. (Color online) Band structure of CdX ($X = \text{O}, \text{S}, \text{Se}, \text{Te}$) within the ACBN0 (red lines) method for the stable rs and zb phase. The PBE (black lines) band structure is also shown for comparison. Brillouin zone integration follows the AFLOW standard as discussed in Ref. [63].

of Zn and Cd that are just below (or little hybridized) with the oxygen and chalcogen p states forming the manifolds at the top of the valence band. The conduction band is dominated by the cation s states. As we proceed from S to Te, the chalcogen p states shift up in energy and this results in the disentangling of the d bands. Compared to ZnS, in CdS the Cd d bands are already well separated from the S p bands. As seen from the PBE band structures, in both ZnO and CdO the d states are more dispersed compared to the chalcogenides. The presence of a spurious p - d hybridization in ZnO is a macroscopic manifestation of the inadequacy of traditional (semi)local functionals to predict correctly the electronic properties of materials where strong electron localization is present and results in the strong underestimation of the band gap: 0.85 eV versus an experimental value of 3.4 eV. Finally, CdO is predicted to be a semimetal by PBE. As it is clearly evident from the figures, the ACBN0 bands (red lines) maintain their overall character as discussed above but display a much wider separation between valence and conduction bands. The relative position of the d bands is shifted to lower energies, thus promoting the disentanglement of the Zn d and O p manifolds. For instance, the ACBN0 converged values for ZnO and CdO energy gaps are 2.91 and 0.70 eV, respectively, in better agreement with the experimental values of 3.4 and 0.9 eV. At the same time, the Zn d bands of ZnO are shifted by approximately 4 eV with respect to the O p bands, removing the spurious hybridization present in PBE (Table VI and Fig. 3).

Note that the ACBN0 follows the HSE functional in predicting the band gaps. Both the ACBN0 and the hybrid

TABLE VI. Average band energies (E_d) in eV for the eight compounds in their stable phases as calculated by PBE, ACBN0, and HSE functionals. The experimental values are taken from Ref. [8]. For CdO, the value is taken from Ref. [48].

Compound	PBE	HSE	ACBN0	Experiment
ZnO	-5.5	-6.2	-9.3	-7.8
ZnS	-6.0	-7.5	-11.7	-9.0
ZnSe	-6.5	-7.5	-12.9	-9.4
ZnTe	-7.0	-8.0	-13.8	-9.8
CdO	-5.5	-6.8	-9.5	-8.7
CdS	-7.0	-7.4	-12.0	-9.6
CdSe	-7.8	-8.0	-13.0	-10.0
CdTe	-8.3	-8.4	-14.0	-10.5

functionals reduce the static correlation energy associated with the localized orbitals and hence provide a similar correction. Indeed, Ivady *et al.* [62] have recently shown that the hybrid exchange correlation potential can be rewritten mathematically as an on-site Hubbard potential for a system of localized orbitals, thus providing a formal justification for our observations.

In Fig. 2(d) we have plotted the error bar in the position of the d manifold of Zn and Cd in PBE, HSE, and ACBN0. We

TABLE VII. Calculated frequencies of optic and acoustic phonons at specific high-symmetry points in the Brillouin zone. We report result computed with ACBN0 and PBE functionals for all the II-VI semiconductors. Comparison with experiments is also reported wherever available. Experimental data are from Refs. [67] (CdTe), [66] (CdO), [64] (ZnSe, ZnS).

System	Mode	PBE	ACBN0	Experiment
ZnS	TO(Γ)	259	266	273
	LO(Γ)	329	364	344
	TO(X)	293	301	312
	LO(X)	309	327	326
	TO(L)	273	280	286
	LO(L)	319	337	333
ZnSe	TO(Γ)	199	198	213
	LO(Γ)	240	260	254
	TO(X)	204	203	216
	LO(X)	204	203	225
	TO(L)	201	200	222
	LO(L)	205	210	236
ZnTe	TO(Γ)	170	172	175
	LO(Γ)	198	213	204
	TO(X)	164	168	183
	LO(X)	174	182	181
	TO(L)	167	170	171
	LO(L)	168	177	177
CdO	TO(Γ)	234	251	266
	LO(Γ)	410	462	465
CdTe	TO(X)	290	325	331
	TO(Γ)	132	134	138
CdTe	LO(Γ)	158	171	167
	TO(X)	137	140	
	LO(X)	137	140	147
	TO(L)	133	137	
CdTe	LO(L)	134	141	142

TABLE VIII. High frequency (ϵ_∞) dielectric constant and Born effective charges (Z) of the II-VI compounds computed with ACBN0 and PBE. The experimental data are from Refs. [64–67].

System	ϵ_∞			Z		
	PBE	ACBN0	Experiment	PBE	ACBN0	Experiment
ZnS	5.98	4.12	5.13	2.02	2.10	2.1
ZnSe	7.40	4.98	5.70	2.12	2.17	2.21
ZnTe	9.38	6.01	7.2	2.22	2.19	2.0
CdO	7.13	3.52	5.3	2.40	1.97	
CdTe	9.13	5.56	7.1	2.45	2.34	2.06

clearly observe the limits of ACBN0 and HSE in predicting the energy of the d bands relative to the valence band maximum. In PBE and HSE we see a negative error of around 40%, which indicates that the position of the d bands are higher in energy compared to the experimental values, while in ACBN0 the bands are pushed much lower, closer to the experimental position. The reason for the overestimation of the d band energy in HSE calculations is due to the incomplete treatment of correlation energy of the localized d electrons. In ACBN0, downward shifting of the $3d$ or $4d$ bands increase monotonically with increasing values of U_{eff} . The rigid shift of the bands arises from a singularity due to the filled character of the d^{10} bands and it is implicit in the definition of the Hubbard correction. An extensive discussion for the case of ZnO is provided in Ref. [29].

C. Lattice dynamical properties

In the wide band-gap semiconductors, the incorrect description of the covalency of the cation-anion bond affects the electrostatic properties of the system and, consequently, the phonon distribution and the coupling with the external fields. This problem is more pronounced in the oxides compared to the chalcogenides. In ZnO the underestimated band gap within PBE functionals leads to an overestimate of the high-frequency dielectric constant (ϵ_∞) and, in turn, a large discrepancy in the LO-TO splitting. The PBE value of 5.24 is higher compared to the experimental value of 3.14 [37]. Similarly, in CdO the PBE dielectric constant is 7.13 compared to the experimental value

of 5.3. This trend of overestimation of the high-frequency dielectric constant is observed in the other chalcogenides as well.

The ACBN0 functional provides a proper description of the electronic and structural features of the II-VI semiconductors and improves the dielectric and vibrational properties leading, in most cases, to smaller deviations with respect to the experimental data. The calculated high frequency dielectric constants (ϵ_∞), the Born effective charges (Z^*), and the zone-center phonon frequencies are summarized in Tables VII and VIII. We did not find any references to vibrational properties calculated within the HSE method which is computationally very expensive especially for calculating the response functions.

In this section we also show the accuracy of the phonon spectrum for six representative compounds: ZnS, ZnSe, ZnTe, CdO, CdS, and CdTe. ACBN0 phonons frequencies are compared with the PBE and experimental values. The dielectric properties and the vibrational spectrum of the II-VI semiconductors were calculated using a coupled finite-fields/finite differences approach as discussed extensively in Ref. [37]. The PBE and ACBN0 phonon dispersions are reported in Figs. 5 and 6. In the Zn chalcogenides the acoustic manifold is equally well reproduced within the PBE and the ACBN0 formalisms (deviations of few cm^{-1} with respect to the available experimental data). For the optic manifold, however, ACBN0 improves the agreement with experiment. This result may be rationalized in terms of the more accurate description of the bonding. In both CdO and CdTe, the ACBN0 values are in excellent agreement with the experiments and improve the PBE description especially for the optic manifolds. In CdS both ACBN0 and PBE are in good agreement with the experiments.

IV. CONCLUSIONS

The procedure to compute from first principles the Hubbard correction as implemented in the ACBN0 functional largely improves the electronic structure with respect to PBE. The energy band gap in Cd and Zn oxides and chalcogenides computed within the ACBN0 formalism is very close to the value computed with hybrid functional at a computational cost of roughly 10%. The ACBN0 functional generally improves the structural and the vibrational parameters reaching improved

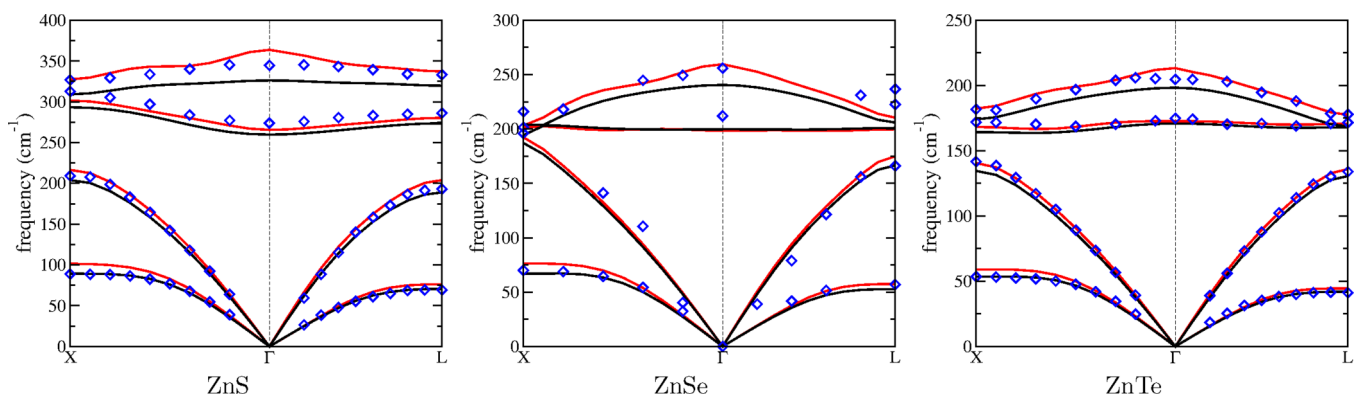


FIG. 5. (Color online) Phonon dispersion of ZnX ($X = \text{S}, \text{Se}, \text{Te}$) within the ACBN0 method for the zb phase (red). The PBE phonon dispersions (black) is also shown for comparison. Open blue diamonds represent inelastic scattering data from Refs. [64,65]. We show only the directions in the Brillouin zone that have been measured, see the Supplemental Material [32] for the full phonon dispersions.

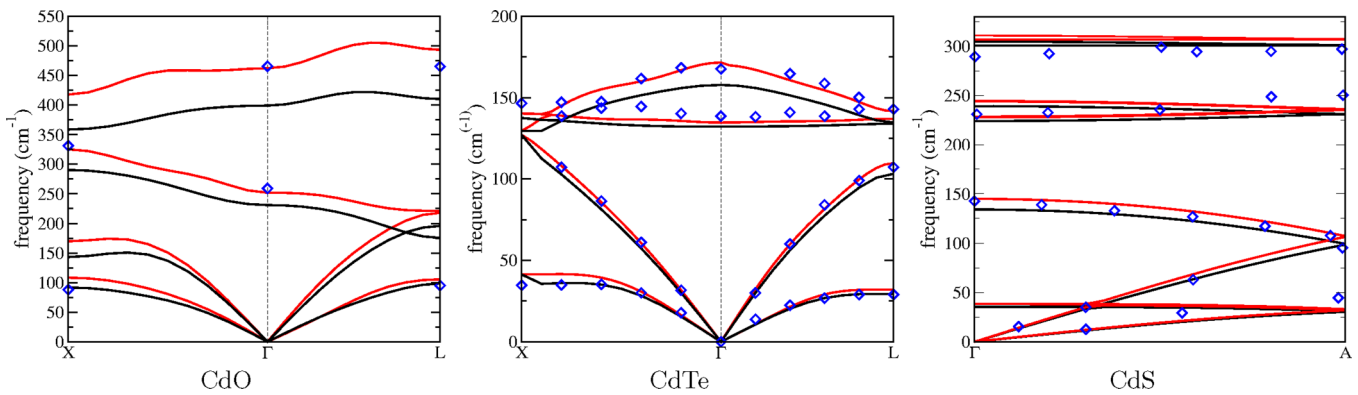


FIG. 6. (Color online) Calculated phonon dispersion of CdX ($X = O, S, Te$) within the ACBN0 (red lines) and PBE (black lines) method for the zb phase. Open blue diamonds represent experiment inelastic neutron scattering data are from Refs. [66,67]. We show only the directions in the Brillouin zone that have been measured, see the Supplemental Material [32] for the full phonon dispersions.

agreement with the experiments. Both hybrid functionals and ACBN0 have limited predictive value when considering the position of the occupied d manifolds, at least in ZnS, ZnSe, ZnTe, ZnO, CdS, CdSe, CdTe, and CdO that we investigated.

ACKNOWLEDGMENTS

We thank A. Calzolari, H. Shi, I. Takeuchi, G. Hart, and R. Forcade for various technical discussions that have contributed

to the results reported in this article. This work was supported by ONR-MURI under Contract N00014-13-1-0635, DOD-ONR (N00014-14-1-0526), and the Duke University Center for Materials Genomics. S.C. acknowledges partial support by DOE (DE-AC02-05CH11231, BES program under Grant No. EDCBEE). We also acknowledge the Texas Advanced Computing Center (TACC) at the University of Texas Austin for providing HPC resources, and the CRAY corporation for computational assistance.

- [1] J. Wang and M. Isshiki, in *Springer Handbook of Electronic and Photonic Materials*, edited by S. Kasap and P. Capper (Springer, New York, 2007), pp. 325–342.
- [2] J. P. Perdew and A. Zunger, *Phys. Rev. B* **23**, 5048 (1981).
- [3] J. P. Perdew, K. Burke, and M. Ernzerhof, *Phys. Rev. Lett.* **77**, 3865 (1996).
- [4] A. Mang, K. Reimann, and S. Rübenacke, *Solid State Commun.* **94**, 251 (1995).
- [5] R. A. Powell, W. E. Spicer, and J. C. McMenamin, *Phys. Rev. B* **6**, 3056 (1972).
- [6] A. Schleife, F. Fuchs, J. Furthmüller, and F. Bechstedt, *Phys. Rev. B* **73**, 245212 (2006).
- [7] I. N. Demchenko, J. D. Denlinger, M. Chernyshova, K. M. Yu, D. T. Speaks, P. Olalde-Velasco, O. Hemmers, W. Walukiewicz, A. Derkachova, and K. Lawniczka-Jablonska, *Phys. Rev. B* **82**, 075107 (2010).
- [8] D. Vogel, P. Krüger, and J. Pollmann, *Phys. Rev. B* **54**, 5495 (1996).
- [9] L. Ley, R. A. Pollak, F. R. McFeely, S. P. Kowalczyk, and D. A. Shirley, *Phys. Rev. B* **9**, 600 (1974).
- [10] J. P. Perdew and M. Levy, *Phys. Rev. Lett.* **51**, 1884 (1983).
- [11] L. J. Sham and M. Schluter, *Phys. Rev. Lett.* **51**, 1888 (1983).
- [12] J. P. Perdew, R. G. Parr, M. Levy, and J. L. Balduz, Jr., *Phys. Rev. Lett.* **49**, 1691 (1982).
- [13] V. I. Anisimov, F. Aryasetiawan, and A. I. Lichtenstein, *J. Phys.: Condens. Matter* **9**, 767 (1997).
- [14] A. I. Lichtenstein, V. I. Anisimov, and J. Zaanen, *Phys. Rev. B* **52**, R5467 (1995).
- [15] F. Aryasetiawan and O. Gunnarsson, *Rep. Prog. Phys.* **61**, 237 (1998).
- [16] F. Fuchs, J. Furthmüller, F. Bechstedt, M. Shishkin, and G. Kresse, *Phys. Rev. B* **76**, 115109 (2007).
- [17] M. Shishkin and G. Kresse, *Phys. Rev. B* **75**, 235102 (2007).
- [18] J. Heyd, G. E. Scuseria, and M. Ernzerhof, *J. Chem. Phys.* **118**, 8207 (2003).
- [19] J. Heyd, G. E. Scuseria, and M. Ernzerhof, *J. Phys. Chem.* **124**, 219906 (2006).
- [20] B. Himmetoglu, A. Floris, S. de Gironcoli, and M. Cococcioni, *Int. J. Quantum Chem.* **114**, 14 (2014).
- [21] M. Springer and F. Aryasetiawan, *Phys. Rev. B* **57**, 4364 (1998).
- [22] O. Gunnarsson, O. K. Andersen, O. Jepsen, and J. Zaanen, *Phys. Rev. B* **39**, 1708 (1989).
- [23] M. Cococcioni and S. de Gironcoli, *Phys. Rev. B* **71**, 035105 (2005).
- [24] S. Kümmel and L. Kronik, *Rev. Mod. Phys.* **80**, 3 (2008).
- [25] Editorial, *Nat. Mater.* **12**, 173 (2013).
- [26] L. A. Agapito, A. Ferretti, A. Calzolari, S. Curtarolo, and M. Buongiorno Nardelli, *Phys. Rev. B* **88**, 165127 (2013).
- [27] S. Curtarolo, G. L. W. Hart, M. Buongiorno Nardelli, N. Mingo, S. Sanvito, and O. Levy, *Nat. Mater.* **12**, 191 (2013).
- [28] R. H. Taylor, F. Rose, C. Toher, O. Levy, K. Yang, M. Buongiorno Nardelli, and S. Curtarolo, *Comp. Mater. Sci.* **93**, 178 (2014).
- [29] L. A. Agapito, S. Curtarolo, and M. Buongiorno Nardelli, *Phys. Rev. X* **5**, 011006 (2015).
- [30] S. L. Dudarev, G. A. Botton, S. Y. Savrasov, C. J. Humphreys, and A. P. Sutton, *Phys. Rev. B* **57**, 1505 (1998).
- [31] A. N. Andriotis, G. Mpourmpakis, S. Lisenkov, R. M. Sheetz, and M. Menon, *Phys. Status Solidi (b)* **250**, 356 (2013).

- [32] See Supplemental Material at <http://link.aps.org/supplemental/10.1103/PhysRevB.91.245202> for Band structures and DOS plots reported.
- [33] P. Giannozzi, S. Baroni, N. Bonini, M. Calandra, R. Car, C. Cavazzoni, D. Ceresoli, G. L. Chiarotti, M. Cococcioni, I. Dabo, A. Dal Corso, S. de Gironcoli, S. Fabris, G. Fratesi, R. Gebauer, U. Gerstmann, C. Gougoussis, A. Kokalj, M. Lazzeri, L. Martin-Samos, N. Marzari, F. Mauri, R. Mazzarello, S. Paolini, A. Pasquarello, L. Paulatto, C. Sbraccia, S. Scandolo, G. Sclauzero, A. P. Seitsonen, A. Smogunov, P. Umari, and R. M. Wentzcovitch, *J. Phys.: Condens. Matter* **21**, 395502 (2009).
- [34] A. Calzolari, N. Marzari, I. Souza, and M. Buongiorno Nardelli, *Phys. Rev. B* **69**, 035108 (2004).
- [35] See, for instance, WanT code by A. Ferretti, B. Bonferroni, A. Calzolari, and M. Buongiorno Nardelli, <http://www.wannier-transport.org>.
- [36] G. Kresse and J. Furthmüller, *Phys. Rev. B* **54**, 11169 (1996).
- [37] A. Calzolari and M. Buongiorno Nardelli, *Sci. Rep.* **3**, 2999 (2013).
- [38] J. Hong, A. Stroppa, J. Íñiguez, S. Picozzi, and D. Vanderbilt, *Phys. Rev. B* **85**, 054417 (2012).
- [39] Springer Materials: The Landolt-Börnstein Database, <http://www.springermaterials.com/docs/index.html>.
- [40] A. Ashrafi and C. Jagadish, *J. Appl. Phys.* **102**, 071101 (2007).
- [41] J. Uddin and G. E. Scuseria, *Phys. Rev. B* **74**, 245115 (2006).
- [42] C. Fan, Q. Wang, L. Li, S. Zhang, Y. Zhu, X. Zhang, M. Ma, R. Liu, and W. Wang, *Appl. Phys. Lett.* **92**, 101917 (2008).
- [43] M. Grünwald, A. Zayak, J. B. Neaton, P. L. Geissler, and E. Rabani, *J. Chem. Phys.* **136**, 234111 (2012).
- [44] J. E. Jaffe, R. Pandey, and M. J. Seel, *Phys. Rev. B* **47**, 6299 (1993).
- [45] J. Heyd, J. E. Peralta, G. E. Scuseria, and R. L. Martin, *J. Chem. Phys.* **123**, 174101 (2005).
- [46] N. Lakshmi, N. M. Rao, R. Venugopal, D. Reddy, and B. Reddy, *Mater. Chem. Phys.* **82**, 764 (2003).
- [47] M. Burbano, D. O. Scanlon, and G. W. Watson, *J. Am. Chem. Soc.* **133**, 15065 (2011).
- [48] J. J. Mudd, T.-L. Lee, V. Muñoz-Sanjosé, J. Zúñiga-Pérez, D. J. Payne, R. G. Egdell, and C. F. McConville, *Phys. Rev. B* **89**, 165305 (2014).
- [49] L. Shi, Y. Qin, J. Hu, Y. Duan, L. Qu, L. Wu, and G. Tang, *Europhys. Lett.* **106**, 57001 (2014).
- [50] Y. Hinuma, F. Oba, Y. Kumagai, and I. Tanaka, *Phys. Rev. B* **88**, 035305 (2013).
- [51] E. H. Kisi and M. M. Elcombe, *Acta Crystallogr. Sect. C* **45**, 1867 (1989).
- [52] H. Liu, J. S. Tse, and H.-k. Mao, *J. Appl. Phys.* **100**, 093509 (2006).
- [53] F.-G. Kuang, X.-Y. Kuang, S.-Y. Kang, M.-M. Zhong, and A.-J. Mao, *Mater. Sci. Semicond. Process.* **23**, 63 (2014).
- [54] S. Yadav and R. Ramprasad, *Appl. Phys. Lett.* **100**, 241903 (2012).
- [55] S. Kasap and P. Capper, *Springer Handbook of Electronic and Photonic Materials* (Springer, New York, 2007).
- [56] R. Peverati and D. G. Truhlar, *J. Chem. Phys.* **136**, 134704 (2012).
- [57] Q. Yan, P. Rinke, M. Winkelnkemper, A. Qteish, D. Bimberg, M. Scheffler, and C. G. Van de Walle, *Appl. Phys. Lett.* **101**, 152105 (2012).
- [58] A. Janotti, D. Segev, and C. G. Van de Walle, *Phys. Rev. B* **74**, 045202 (2006).
- [59] S. K. Vasheghani Farahani, V. Muñoz-Sanjosé, J. Zúñiga-Pérez, C. F. McConville, and T. D. Veal, *Appl. Phys. Lett.* **102**, 022102 (2013).
- [60] U. Rossow, T. Werninghaus, D. Zahn, W. Richter, and K. Horn, *Thin Solid Films* **233**, 176 (1993).
- [61] H. Xiao, J. Tahir-Kheli, and W. A. Goddard III, *J. Phys. Chem. Lett.* **2**, 212 (2011).
- [62] V. Ivády, R. Armiento, K. Szász, E. Jánzén, A. Gali, and I. A. Abrikosov, *Phys. Rev. B* **90**, 035146 (2014).
- [63] W. Setyawan and S. Curtarolo, *Comp. Mater. Sci.* **49**, 299 (2010).
- [64] B. Hennion, F. Moussa, G. Pepy, and K. Kunc, *Phys. Lett. A* **36**, 376 (1971).
- [65] N. Vagelatos, D. Wehe, and J. King, *J. Chem. Phys.* **60**, 3613 (1974).
- [66] R. Oliva, J. Ibáñez, L. Artús, R. Cuscó, J. Zúñiga-Pérez, and V. Muñoz-Sanjosé, *J. Appl. Phys.* **113**, 053514 (2013).
- [67] J. Rowe, R. Nicklow, D. Price, and K. Zanio, *Phys. Rev. B* **10**, 671 (1974).